Estimating Respiratory Motion from Cone-Beam Projections

Jef Vandemeulebroucke[1,2,3], Patrick Clarysse[1], Jan Kybic[3], and David Sarrut[1,2]

[1] Université de Lyon, Creatis-LRMN Laboratory, INSA-Lyon, France
[2] Université de Lyon, Centre Léon Bérard, 28 rue Laennec, 69353 Lyon, France
[3] Center For Machine Perception, Czech Technical University, Prague, Czech Republic

Abstract. Respiratory motion introduces uncertainties when planning and delivering radiotherapy treatment to lung cancer patients. Cone-beam projections potentially constitute a valuable source of motion information that could serve for motion compensated reconstruction and to learn the relationship between internal motion and respiratory correlated signals. We propose a method for respiratory motion estimation directly from cone-beam projections by including prior knowledge about the patient's breathing motion. The method requires that a four-dimensional computed tomography is available from which a patient specific model is constructed. Each cone-beam projection is compared to cone-beam projection views of the model and motion estimation is accomplished by optimizing the model parameters with respect to a similarity measure. Experiments on simulated data show satisfying results. Experiments on real cone-beam projections are currently being undertaken in order to confirm these observations.

1 Introduction

External beam radiotherapy is the primary treatment modality for patients with non-operable lung cancer. Respiratory motion introduces uncertainties during imaging, treatment planning and treatment delivery [1]. To reduce respiratory motion induced image artifacts, respiratory-correlated acquisition techniques have been developed resulting in four-dimensional computed tomography images (4DCT). These images provide additional information about tumor and organ-at-risk position and trajectory that can be incorporated in the treatment planning process. To account for respiratory motion additional margins are considered during treatment planning and treatment delivery methods such as breath-hold and gating methods have been developed. These methods often use an external respiratory correlated signal such as lung air flow or abdominal height as a surrogate for tumor motion during the actual treatment. Changes of the respiratory motion over the duration of the treatment have been reported [2] and may influence the relationship between tumor motion and surrogate. Recent developments have made cone-beam CT (CBCT) mounted on the linear accelerator [3] available, which makes it possible to acquire patient images in treatment

position just prior to treatment. As with conventional CT, three-dimensional (3D) CBCT is heavily influenced by respiratory motion. Respiratory correlated CBCT [4] reduces respiratory motion artifacts. However, seeing only a subset of the CB projections is used to reconstruct each 3D CBCT image, the resulting image quality is lower. Motion compensated CB reconstruction techniques [5], [6] have been proposed enabling the use of all the acquired projections. These methods however require knowledge of the motion present during CB acquisition.

CB projections are potentially a valuable source of motion information that could be used for motion compensated reconstruction and to study the relationship between an external surrogate signal and tumor motion. Zijp *et al.* [7] proposed a fast and robust method to extract the breathing phase from a sequence of CB projections of the thorax. The method produces a breathing signal from which the phase can be derived and has been successfully applied for respiratory correlated CB reconstruction [4]. Zeng *et al.* [8] proposed a method for 3D motion estimation from a sequence of CB projections. A B-spline deformation model is used to deform a reference CT volume to match the motion observed in the CB projections. The applied deformations are optimized by computing the similarity between the CB projection views of the deformed volume and the CB projection sequence. Optimization of the numerous parameters of the B-spline deformation model was regularized by introducing spatial and temporal motion roughness penalties and an aperiodicity penalty for the estimated breathing motion. Results on simulated data were encouraging, demonstrating the feasibility of the approach.

We propose a method for estimating 3D respiratory motion from a CB projection sequence by incorporating prior knowledge about the patient's respiratory motion. The proposed method requires that a 4DCT image of the patient is available at CB acquisition time. From this image the respiratory motion is estimated using deformable registration. The motion estimation is incorporated into a patient specific motion model with two parameters: the breathing phase and amplitude. For each CB projection, the 3D motion estimation comes down to finding the model parameters for which the modeled CB projection view best matches the CB projection with respect to a similarity measure. In the next section the images used and the construction of the patient specific motion model are discussed. Next the proposed cost function and optimization scheme are detailed. Section 3 contains the experiments performed to test the proposed method and the results for these experiments. Section 4 focuses on known limitations and issues related to the chosen approach and outlines future work.

2 Materials and Methods

2.1 4DCT and Deformable Registration

The images used for this study are part of a freely available data set [9]. It consists of a 4DCT image of the thorax composed of 10 3DCT images representing different phases of the respiratory cycle.The data set is completed by 400 anatomical landmarks (40 in each 3DCT image) identified by medical experts.

Each of the 3DCT images will be referred to as a *phase* of the 4DCT. Deformations between the phases were estimated by deformably registering them to one particular phase, arbitrarily chosen to be the end-inhalation phase. Registration was performed using the demons algorithm [10], of which its effectiveness on CT images of the thorax was verified in earlier work by our group [11]. The accuracy of the registrations was assessed using the landmarks provided with the data set. The phase to phase displacements of 40 anatomical points, as estimated by medical experts, were compared to the displacements given by the registration results. The average registration error was thus estimated to be 1.2mm with a standard deviation of 0.4mm. The maximum misalignment for these landmarks was found to be 2.6mm.

2.2 Patient Model

Using the registration results obtained above, we can construct a patient specific motion model. The proposed model is composed of a reference image I_{ref} and a deformation model T. I_{ref} should be *warped* using the deformation model T to obtain a modeled breathing state S. There are at least two ways of warping an image with a deformation field: you can obtain the target through either backward or forward mapping of the source. Suppose we have a source volume I and a target volume J. In addition suppose we have estimated the displacements of voxels of I to their corresponding positions in J and inversely. We can obtain J through backwards mapping of the source voxels:

$$J(\mathbf{x}) = I(\mathbf{x} + D_{J\rightarrow I}(\mathbf{x})) \; . \tag{1}$$

where $D_{J\rightarrow I}(\mathbf{x})$ represents the displacement necessary to map a voxel with position $\mathbf{x}$ in the target space to its corresponding position in the source space. J is thus obtained by fetching for each voxel position of J its corresponding (interpolated) value in I. The second possibility is through forward mapping:

$$J(\mathbf{x} + D_{I\rightarrow J}(\mathbf{x})) = I(\mathbf{x}) \; . \tag{2}$$

where this time $D_{I\rightarrow J}(\mathbf{x})$ represents the displacement necessary to map a voxel with position $\mathbf{x}$ in the source space to its corresponding position in the target space. J is obtained by adding for each voxel position of I, a contribution to the neighboring voxels of its corresponding position in J. If not explicitly taken into account, forward mapping can lead to holes in the target image, i.e. voxels for which no contribution was added. Backwards mapping is usually preferred as it allows for a more efficient implementation.

The reference image for the proposed model is the *mean-position image* (MPI), which we define as the image in which all structures appear at their time-weighted mean position. This concept was also used by Wolthaus *et al.* [12] for the definition of the *mid-ventilation phase*. Note that due to hysteresis of the respiratory motion, the mean position of a moving structure does not necessarily lie on the trajectory of that structure. It was obtained in the following way. For each voxel of the end-inhalation used as reference image for the registrations

described in Section 2.1, we calculated the mean of the deformation vectors mapping this voxel to its positions in the other phases (including a zero vector to account for the position of the voxel in the end-inhalation phase itself). The end-inhalation phase was then deformed using this mean deformation field, through backwards mapping. This requires the inversion of the mean deformation field. The Figure 1 shows a graphical representation of the MPI.

The second element in the patient model is the deformation model T allowing I_{ref} to be warped to a different breathing state. As we want to incorporate the phase to phase deformations observed in the 4DCT image, T should at least be able to reach these states. The deformations between the MPI and the phases of the 4DCT were again estimated through deformable registration. It was preferred to re-estimated the deformations to avoid accumulating errors by composing the previously obtained deformation fields. The resulting deformation fields were combined to form a 4D vector image, the fourth dimension being the breathing phase ϑ. This vector image was recursively filtered to obtain a 4D continuous cubic B-spline representation [13], denoted by $T(\mathbf{x}, \vartheta)$. In addition to modelling the phase to phase deformations, a second model parameter α was introduced to allow inter- and intracyle variations of the deformations. α can be interpreted as an instantaneous amplitude, linearly scaling the displacements of all voxels given by T for a certain value of ϑ.

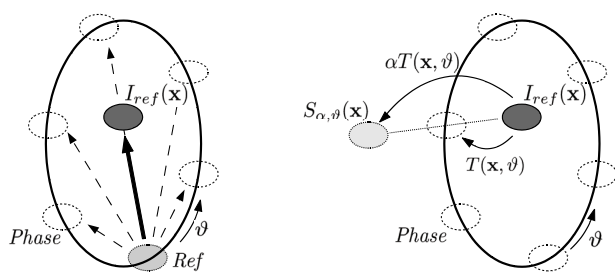

Fig. 1. (a) Schematic 2D representation of the construction of the MPI. A reference phase of the 4DCT (*Ref*) is registered to all other phases. For each voxel the estimated displacements are averaged (*bold arrow*) and after inversion used to obtain $I_{ref}(\mathbf{x})$ through backwards mapping of the reference phase. (b) Schematic 2D representation of the patient model. An anatomical point of I_{ref} is shown at its time-weighted mean position $\mathbf{x}$. Its corresponding position in the phases of the 4DCT was estimated through deformable registration. Interpolating these positions yields the closed contour represented in bold, which can be interpreted as an estimated trajectory. $T(\mathbf{x}, \vartheta)$ will map $\mathbf{x}$ on this trajectory, whereas $\alpha T(\mathbf{x}, \vartheta)$ can map $\mathbf{x}$ to any breathing state $S_{\vartheta,\alpha}(\mathbf{x})$ in the plane of the ellipse.

Backwards mapping I_{ref} using T would require to use the deformations defined from the space of the phases of the 4DCT (the target volumes) to I_{ref} (the source volume). In this case interpolating these deformation fields with a cubic spline would be interpolating the end point of vectors which have different starting positions. Similarly, when scaling the deformations by α, one should scale the deformations defined from I_{ref} to the phases of the 4DCT. Tests were performed performed with both backwards and forward mapping and showed very little difference to the resulting target volumes and especially to their CB projection view. This is due to the fact that the deformation fields vary quite smoothly in space. In this work forward mapping was used when warping I_{ref} to S. With $T(\mathbf{x}, \vartheta)$ representing the deformation given by the cubic spline for a phase ϑ on position $\mathbf{x}$, we can represent a model breathing state S through forward mapping as:

$$S(\mathbf{x} + \alpha T(\mathbf{x}, \vartheta)) = I_{ref}(\mathbf{x}) \ . \tag{3}$$

We will use $S_{\vartheta,\alpha}$ to represent the image that is the result of deforming I_{ref} through forward mapping using the deformations as given by $\alpha T(\mathbf{x}, \vartheta)$. The phase parameter $\vartheta \in [0, 1[$, goes through all breathing phases from the end-exhale phase to end-inhale and back to end-exhale when rising from 0 to 1. For the parameters at values $\alpha = 1$ and $\vartheta = 0, 0.1, 0.2, ...$ the modeled breathing states correspond to the phases of the 4DCT. For $\alpha = 0$, I_{ref} is found. The right panel of Figure 1 shows a schematic representation of the proposed patient model.

2.3 Cost Function and Optimization

In order to compare the 3D modeled breathing state $S_{\vartheta,\alpha}$ to a CB projection p_ϕ taken from a projection angle ϕ, we calculate its CB projection view. Let $\mathcal{A}_\phi$ denote the ideal CB projection operator from a projection angle ϕ. The projection operator $\mathcal{A}_\phi$, was made to simulate the geometry of the Elekta Synergy. Figure 2 shows the modeled CB projection view of I_{ref}. For comparison we also show a CB projection of the same patient acquired on the Elekta Synergy. The horizontal object present in the CB projection is a reinforcement of the treatment table. For each CB projection can define the optimization problem as follows:

$$(\hat{\vartheta}, \hat{\alpha})_\phi = arg \max_{\vartheta,\alpha}(\mathcal{F}(p_\phi, \mathcal{A}_\phi S_{\vartheta,\alpha})) \ . \tag{4}$$

where $\hat{\vartheta}$ and $\hat{\alpha}$ represent the estimated model parameters, $\mathcal{F}(.,.)$ is a similarity measure for which we assumed that higher values correspond to higher similarity. The optimization is performed in the space of the model parameters with respect to the similarity measure between the real projection and the modeled projection view. We used mutual information as similarity measure [14]. The cost function was handed to a Powell optimization strategy [15]. Each subsequent optimization was initialized with the model parameters found for the previous CB projection.

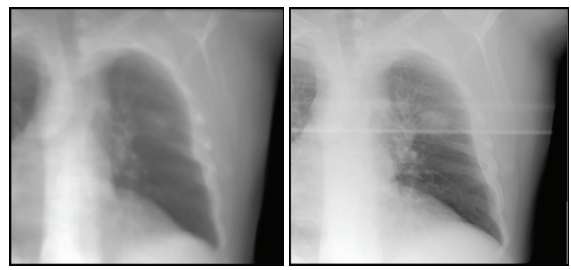

(a) (b)

Fig. 2. (a) CB projection view of I_{ref} and (b) CB projection of the same patient acquired on the Elekta Synergy.

3 Experiments and Results

Validation of the motion estimation on real CB sequences is difficult as no ground truth is available. In this work experiments were performed on a simulated sequence of CB projections. We randomly generated a continuous phase signal with a varying period using the statistical properties reported for the breathing period by George *et al.* [16]. This resulted in a breathing period that varied between 2.2s and 5.6s. The phase was not limited to linear functions of time, allowing for intracycle breath rate variations. The continuous amplitude signal α was randomly generated using a lognormal random number generator, and was limited to slow variations in time and values close to one. The thus obtained amplitude signal varied between 0.88 and 1.21. These parameter values were fed to the patient model and the CB projection views were calculated every 0.6°, twice per second and starting from the right lateral side of the patient. This is in good correspondence with actual CB acquisition parameters. We ran the proposed method for the first 150 projections, which amounts to 30 seconds of scanning time over an angle of 90°. The optimization for the first projection was initialized with $\vartheta = 0$ and $\alpha = 1$ which was close to the generated values $\vartheta = 0.02$, $\alpha = 1.1$. It is our opinion that including a second parameter to account for the inter- and intracycle variations of amplitude extents the grasp of the method and makes the estimation of the phase more robust. To verify this we ran the optimization a second time on the same generated CB projection sequence but now fixing the amplitude of the patient model to one. The phase estimated using this method will be noted as $\breve{\vartheta}$. Results obtained through this method will be referred to as estimated using a *phase based model* (PhM), as opposed to using the *phase-amplitude based model* (PhAM). The generated phase signal and amplitude signal of the simulated CB sequence and their estimated values are shown in Figure 3 in function of the projection number. The estimation errors are summarized for the whole CB sequence in Table 1. We also assessed the 3D misalignment for the landmarks discussed in Section 2.1.

Their 3D positions in the breathing states used to generate the CB sequence are compared to their estimated positions. Figure 4 shows the misalignment in function of the projection number while Table 2 summarizes these measures for the whole CB sequence. Figure 5 shows an example of a generated CB projection for which difference images where calculated with the CB projection view of I_{ref} and with the estimated CB projections. For this projection (with projection number 138), estimation errors were around their average value. When running the optimization with the PhAM, results are accurate for the entire sequence, yielding acceptable maximum errors and excellent mean errors for parameter value. Figure 4 shows that the maximum misalignment of up to 16mm was effectively reduced to below 1mm for this experiment. When using the PhM, the phase estimate showed bad correspondence. With respect to the 3D misalignment, the estimated sequence hardly improved the mean misalignment of the landmarks with respect to before the optimization.

Table 1. Summary of the estimation errors for the parameter values. The table contains the mean absolute estimation error (ME), its standard deviation (SD) and the maximum absolute estimation error ($MaxE$). $\hat{\vartheta}$ and $\hat{\alpha}$ represent the estimates of the model parameters when using a PhAM, $\breve{\vartheta}$ is the phase estimate when PhM.

Parameters	ME	SD	MaxE
$\hat{\vartheta}$	0.0024	0.0265	0.0350
$\hat{\alpha}$	0.0040	0.0001	0.0605
$\breve{\vartheta}$	0.1109	0.2074	0.4800

Table 2. The 3D position of the landmarks is compared to their position in: I_{ref} (*before*), the estimated sequence when using a PhM and the estimated sequence when using a PhAM. The table contains the mean of the misalignment ($MeanM$), its standard deviation (SD) and the maximum misalignment($MaxM$).

Method	MeanM (mm)	SD (mm)	MaxE (mm)
before	3.8544	2.1760	16.7856
PhM	3.5033	1.7747	12.6477
PhAM	0.0184	0.0366	0.9596

4 Discussion and Conclusions

Motion estimation using a phase-amplitude based model performed well on this simulated data. It was expected that the estimates when using a PhM would be

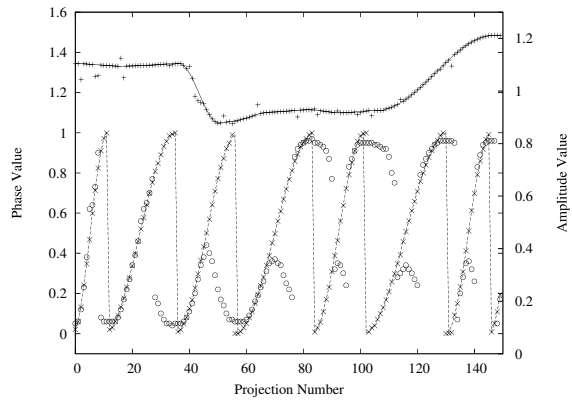

Fig. 3. The randomly generated amplitude signal α (*full line*) and phase signal ϑ (*dashed line*) used to generate the CB projection sequence, and the estimated amplitude $\hat{\alpha}$ (*plus marks*) and phase $\hat{\vartheta}$ (*cross marks*) when using a PhAM. The phase $\breve{\vartheta}$ that was obtained using a PhM is shown in the same graph (*circles*).

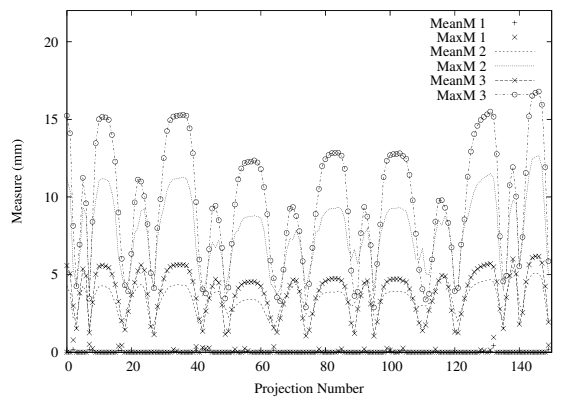

Fig. 4. The 3D position of the landmarks is compared to the their position in the estimated CB projection. The mean and maximum misalignment with the I_{ref} or before optimization (*MeanM 3, MaxM 3*), with the estimated sequence when using a PhM (*MeanM 2, MaxM 2*), with the estimated sequence when using a PhAM (*MeanM 1, MaxM 1*)

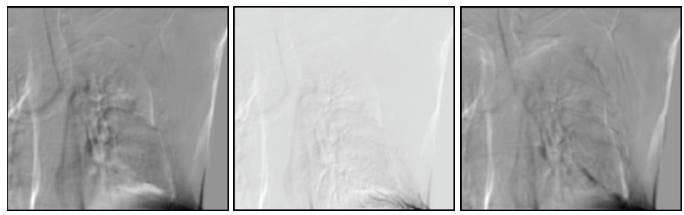

Fig. 5. Difference images between the generated CB projection and the: (*left*) CB projection view of I_{ref}, (*middle*) modeled CB projection view after optimization using the PhAM, (*right*) modeled CB projection view after optimization using the PhM. For the middle image the windowing was altered the emphasize the present differences.

less accurate since the CB sequence was generated using a PhAM. The phase estimates when using a PhM were however surprisingly bad. They indicate that the phase estimation is highly sensitive to even relatively small changes in amplitude. We are currently working on expanding the method for real CB projection sequences. One major issue is validation as it is hard to quantify the accuracy of the motion estimation in the absence of a ground truth. Some other remarks regarding real CB sequences can be made. In order to create CB projection views from the patient model, one must first be able to accurately reproduce the CB geometry and place the patient model in the same physical location as the patient. This can be done by rigidly registering the reconstructed 3D CBCT volume to for example a phase of the 4DCT. Although this CT-CBCT registration should not pose a problem, preliminary tests have shown that the method is highly sensitive to misalignment of the volumes, becoming unpredictable even for small misalignments. In the experiments performed, the similarity measure used showed reliable identification of the optimal parameters on the simulated data, and proved relatively easy to optimize. However several elements could undermine its efficiency when confronted with real CB data. For example, the borders of the treatment table will appear in a large part of the CB projections. Scatter and detector noise, not taken into account by the ideal projection operator, might turn the similarity measure less reliable and harder to optimize. Finally it is possible that changes of the patient anatomy and breathing motion over the course of the treatment are too large to remain adequately represented by the proposed patient model. An example of such changes are baseline shifts (variations of the mean tumor position), which have been reported for lung tumors [2]. The proposed patient model might not handle well large baseline shifts, but can in that case be expanded so that they are explicitly taken into account.

References

1. Keall, P.J., Mageras, G.S., Balter, J.M., Emery, R.S., Forster, K.M., Jiang, S.B., Kapatoes, J.M., Low, D.A., Murphy, M.J., Murray, B.R., Ramsey, C.R., van Herk,

M.B., Vedam, S.S., Wong, J.W., Yorke, E.: The management of respiratory motion in radiation oncology report of AAPM task group 76. Med Phys **33**(10) (Oct 2006) 3874–3900
2. Sonke, J.J., Lebesque, J., van Herk, M.: Variability of four-dimensional computed tomography patient models. Int J Radiat Oncol Biol Phys (Nov 2007)
3. Jaffray, D.A., Siewerdsen, J., Wong, J.W.: Flat-panel cone-beam computed tomography for image-guided radiation therapy. Int J Radiat Oncol Biol Phys **53**(5) (Aug 2003) 1337–1349
4. Sonke, J., Zijp, L., Remeijer, P., van Herk, M.: Respiratory correlated cone beam CT. Med Phys **32**(4) (Apr 2005) 1176–1186
5. Li, T., Koong, A., Xing, L.: Enhanced 4D cone-beam CT with inter-phase motion model. Med Phys **34**(9) (Sep 2007) 3688–3695
6. Rit, S., Wolthaus, J., van Herk, M., Sonke, J.J.: On-the-fly motion-compensated cone-beam CT using an a priori motion model. In: Medical Image Computing and Computer-Assisted Intervention (MICCAI). Volume 5241., New York, USA (2008) 729–736
7. Zijp, L., Sonke, J., van Herk, M.: Extraction of the respiratory signal from sequential thorax cone-beam X-ray images. In: International Conference on the Use of Computers in Radiation Therapy. (May 2004)
8. Zeng, R., Fessler, J.A., Balter, J.M.: Estimating 3-D respiratory motion from orbiting views by tomographic image registration. IEEE Trans Med Imaging **26**(2) (Feb 2007) 153–163
9. Vandemeulebroucke, J., Sarrut, D., Clarysse, P.: The POPI-model, a point-validated pixel-based breathing thorax model. In: XVth International Conference on the Use of Computers in Radiation Therapy, ICCR. (2007)
10. Thirion, J.P.: Image matching as a diffusion process: an analogy with maxwell's demons. Med Image Anal **2**(3) (Sep 1998) 243–260
11. Sarrut, D., Boldea, V., Ayadi, M., Badel, J., Ginestet, C., Clippe, S., Carrie, C.: Nonrigid registration method to assess reproducibility of breath-holding with ABC in lung cancer. Int J Radiat Oncol Biol Phys **61**(2) (Feb 2005) 594–607
12. Wolthaus, J.W.H., van Herk, M., Muller, S.H., Belderbos, J.S.A., Lebesque, J.V., de Bois, J.A., Rossi, M.M.G., Damen, E.M.F.: Fusion of respiration-correlated pet and ct scans: correlated lung tumour motion in anatomical and functional scans. Phys Med Biol **50**(7) (Apr 2005) 1569–1583
13. Unser, M.: Splines: A perfect fit for signal and image processing. IEEE Signal Processing Magazine **16**(6) (November 1999) 22–38 IEEE Signal Processing Society's 2000 magazine award.
14. Maes, F., Collignon, A., Vandermeulen, D., Marchal, G., Suetens, P.: Multimodality image registration by maximization of mutual information. IEEE Trans Med Imaging **16**(2) (Apr 1997) 187–198
15. Press, W.H., Flannery, B.P., Teukolsky, S.A., Vetterling., W.T.: Numerical Recipes in C. Cambridge University Press, second edition (1992)
16. George, R., Vedam, S.S., Chung, T.D., Ramakrishnan, V., Keall, P.J.: The application of the sinusoidal model to lung cancer patient respiratory motion. Med Phys **32**(9) (Sep 2005) 2850–2861